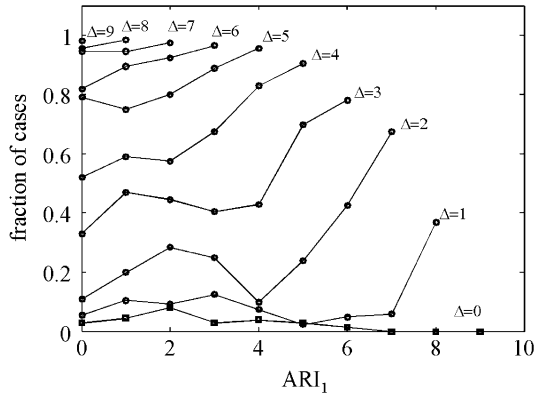

Fig. 2. Simulation results, presenting the fraction of cases in which differences between pairs of estimated ARIs were found to be significant, at the $\boldsymbol{\alpha = 5\%}$ level. The horizontal axis gives the ARI of the first signal ($\mathbf{ARI}_1$, as used in generating the simulated data). That of the second signal $\mathbf{ARI}_2 = \mathbf{ARI}_1 + \boldsymbol{\Delta}$, where $\boldsymbol{\Delta}$ is the difference in the ARIs. $\mathbf{ARI}_1$ and $\mathbf{ARI}_2$ range from 0 to 9, and 200 pairs of signals were simulated.

of the noise estimated from the patient recordings. This was repeated 200 times. The ARI was then estimated for each of the simulated signals, and the bootstrap method applied in order to test the significance of any difference in ARI estimates. The results (Fig. 2) show that, when the "true" ARIs (i.e., the ones corresponding to the filter actually used in generating the simulated signals) are identical ($\Delta = 0$), the expected $\alpha = 5\%$ false positive rate is approximated. However, fewer false positives are detected for $\mathrm{ARI} > 5$, since here the estimator generally finds the correct ARI such that there is no difference in ARI estimates. As the difference between the ARIs increases ($\Delta > 0$), the fraction of cases in which significant differences are found also increases—as expected.

IV. Discussion and Conclusion

The bootstrap method presented provides a relatively simple means for statistical analysis of the ARI. The method is intuitively meaningful, and simulation studies provided further supporting evidence for its use. The results with the patient data indicate that the ARI estimate is not always robust. This had been suspected from the wide variations over time in ARI estimates from the patients, but now the bootstrap method provides confirmation that even within a given recording, ARI estimates can be inconsistent. Short-term variations in autoregulatory activity, nonlinear system characteristics [2], as well as the influence of other physiological variables (e.g., CO_2 and O_2 levels and intracranial pressure variations [1]) on CBFV probably all contribute to the variability of ARI estimates. The proposed bootstrap method now permits quantitative measures (e.g., standard deviation) of the estimation error in the ARIs to be determined, for each recording. This can provide an objective criterion for selecting signals that lead to more robust ARI estimates (e.g., higher variability of ABP and better model fit both were seen to lead to reduced standard deviation), as well as providing a solid basis for the future development of improved filter sets (including nonlinear ones).

While we have applied the proposed bootstrap solution in the analysis of autoregulatory activity, we hope that the method will prove useful in a wider range of problems in constrained system identification for physiological applications.

Acknowledgment

The authors are grateful to Dr. L. Fan for the development of the Doppler system used in this work.

References

[1] O. B. Paulson, S. Strandgaard, and L. Edvinson, "Cerebral autoregulation," *Cerebrovasc. Brain Metab. Rev.*, vol. 2, pp. 161–192, 1990.
[2] R. B. Panerai, "Assessment of cerebral pressure autoregulation in humans—A review of measurement methods," *Phys. Meas.*, vol. 19, pp. 305–338, 1998.
[3] R. B.Panerai, S. L. Dawson, P. J. Eames, and J. F. Potter, "Cerebral blood flow velocity response to induced and spontaneous sudden changes in arterial blood pressure," *Amer. J. Physiol.*, vol. 280, pp. H2162–H2174, 2001.
[4] F. P. Tiecks, A. M. Lam, R. Aaslid, and D. W. Newell, "Comparison of static and dynamic cerebral autoregulation measurements," *Stroke*, vol. 26, pp. 1014–1019, 1995.
[5] D. N. Politis, "Computer intensive methods in statistical analysis," in *IEEE Signal Processing Mag.*, vol. 15, Jan 1998, pp. 39–55.
[6] A. M. Zoubir and B. Boashash, "The bootstrap and its application in signal processing," in *IEEE Signal Processing Mag.*, vol. 15, Jan. 1998, pp. 56–76.
[7] H. Li and G. S. Maddala, "Bootstrapping time series models," *Econometric Rev.*, vol. 15, no. 2, pp. 115–158, 1996.

A Computer-Aided Diagnosis for Distinguishing Tourette's Syndrome From Chronic Tic Disorder in Children by a Fuzzy System With a Two-Step Minimization Approach

Tang-Kai Yin* and Nan-Tsing Chiu

***Abstract*—Tourette's syndrome, no longer considered as a rare and unusual disease, is the most severe tic disorder in children. Early differential diagnosis between Tourette's syndrome and chronic tic disorder is difficult but important because proper and early medical therapy can improve the child's condition. Brain single-photon emission computed tomography (SPECT) perfusion imaging with technetium-99m hexamethylpropylene amine oxime is a method to distinguish these two diseases. In this paper, a fuzzy system called characteristic-point-based fuzzy inference system (CPFIS) is proposed to help radiologists perform computer-aided diagnosis (CAD). The CPFIS consists of SPECT-volume processing, input-variables selection, characteristic-points (CPs) derivation, and parameter tuning of the fuzzy system. Experimental results showed that the major fuzzy rules from the obtained CPs match the major patterns of Tourette's syndrome and chronic tic disorder in perfusion imaging. If any case that was diagnosed as chronic tic by the radiologist but as Tourette's syndrome by the CPFIS was taken as Tourette's syndrome, then the accuracy of the radiologist was increased from 87.5% (21 of 24) without the CPFIS to 91.7% (22 of 24) with the CPFIS. All 17 cases of Tourette's syndrome, which is more severe than chronic tic disorder, were correctly classified. Although the construction and application process of the proposed method is complete, more samples should be used and tested in order to design a universally effective CAD without small sample-size concerns in this research.**

***Index Terms*—AI approaches, biosignal interpretation and diagnostic systems, fuzzy systems, signal and image processing.**

I. Introduction

Tic disorders can be motor tics, vocal tics, or both. They are involuntary, sudden, and repetitive movements or vocalizations. It is esti-

Manuscript received September 9, 2002; revised October 7, 2003. This work was supported in part by the National Science Council under Grant NSC-90-2213-E-041-005. *Asterisk indicates corresponding author.*

*T.-K. Yin is with the Department of Management Information Science, Chia-Nan University of Pharmacy and Science, Tainan, Taiwan, R.O.C. (e-mail: qtkyin@mail.chna.edu.tw).

N.-T. Chiu is with the Department of Nuclear Medicine, College of Medicine, National Cheng Kung University, Tainan, Taiwan, R.O.C.

Digital Object Identifier 10.1109/TBME.2004.827954

mated that 4%–23% of children will exhibit these symptoms [1]. The age of onset of tics varies between 4 and 12 years with a median onset at 7 years [2]. Tourette's syndrome of tic disorders is much more severe than simple tics and chronic motor tics. Besides chronic motor and vocal tics, the patients of Tourette's syndrome may have behavioral disorders, sleep disturbances, headaches, and attention deficit disorders.

The outcome and treatment of Tourette's syndrome and chronic tic disorder are distinct. Early differential diagnosis between these two childhood-onset diseases is difficult but important because proper and early medical therapy can improve the child's condition. It is so difficult that many researches provide warning that some Tourette's syndrome cases may be misdiagnosed [3]–[5].

In this paper, a computer-aided diagnosis (CAD) is proposed to distinguish Tourette's syndrome from chronic tic disorder. Instead of diagnosing behavioral disorders, inspection on brain imaging is taken. Technetium-99m hexamethylpropylene amine oxime (HMPAO) single-photon emission computed tomography (SPECT) brain imaging has been applied to the diagnosis and treatment of Tourette's syndrome and has become a useful tool in aiding radiologists [6], [7]. It is based on the estimation of the regional cerebral blood flows by using technetium-99m labeled to the lipophylic agent, HMPAO [8]. Hypoperfused brain areas can be related to Tourette's syndrome [9], [10]. Visual interpretation or semi-quantitative analysis is conducted by experts to perform perfusion analysis. The aim of the proposed CAD is to act as a second-opinion reader that can assist radiologists in differentiating Tourette's syndrome and chronic tic disorder.

Neural networks, fuzzy systems, and the combination of both have been successfully applied to CAD such as microcalcification detection [11], [12] and lung nodule detection [13]. In this paper, a characteristic-point-based fuzzy inference system (CPFIS) is used to implement the CAD. The CPFIS has been successfully applied to locating abnormalities in bone scintigraphy [14]. A new and more systematic method, gradient-projection method, is proposed to obtain characteristic points (CPs) in this research. It is based on the minimization of approximation errors by adjusting the weights of fuzzy rules. After the training of the proposed system, the obtained CPs can provide major patterns embedded in training data. This pattern information is helpful in understanding specific perfusion differences between Tourette's syndrome and chronic tic disorder. Then this new knowledge can be accumulated into or compared with that of human experts.

In the construction of the proposed fuzzy system, there are three major procedures: SPECT-volume processing, input-variables selection, and fuzzy-system construction. In the SPECT-volume processing, the five data slices around the corpus callosum are selected according to the suggestions of a radiologist (Nan-Tsing Chiu, MD). On the five data slices, 21 left–right regions are obtained and the asymmetry values on these 21 regions are derived for each SPECT volume. After all SPECT volumes are processed, we have a set of 21-input–1-output data. Then these data are further processed by the nearest-point algorithm to be a smaller data set as m-input–1-output training data, $m \leq 21$, which is more suitable for two-class diagnosis. Finally, the training data are processed by a two-step minimization approach: gradient-projection method and back-propagation fine-tuning. The former will decide the number of fuzzy rules, while the latter will fine tune the parameters of these fuzzy rules.

The remainder of this paper is organized as follows. Section II describes the processing of SPECT volumes. The five chosen data slices around the found corpus callosum and 21 asymmetry values on the 21 left–right regions are presented. In Section III, the nearest-point algorithm is employed to choose effective variables among the 21 variables of asymmetry and form m-input–1-output training data, $m \leq 21$. In Section IV, the construction of the fuzzy system is performed in two steps: gradient-projection method and back-propagation fine-tuning.

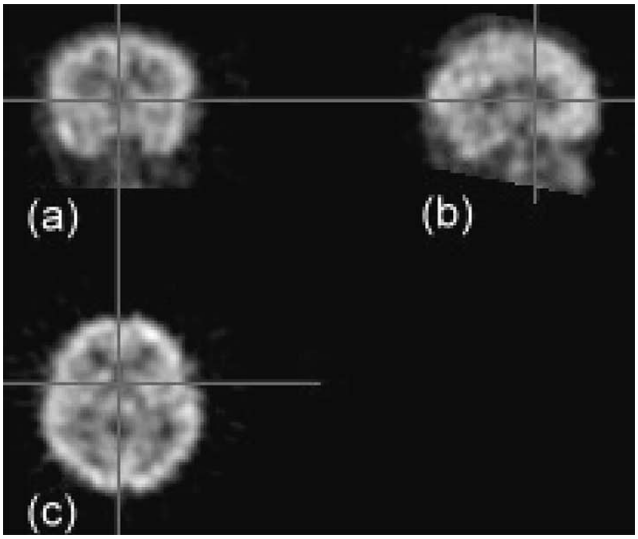

Fig. 1. SPECT sample in the $\boldsymbol{x}$–$\boldsymbol{y}$–$\boldsymbol{z}$ coordinates. (a) Coronal view or $\boldsymbol{x}$–$\boldsymbol{z}$ plane. (b) Sagittal view or $\boldsymbol{y}$–$\boldsymbol{z}$ plane. (c) Transverse view or $\boldsymbol{x}$–$\boldsymbol{y}$ plane.

Experiment results are discussed in Section V. Finally, Section VI concludes this paper.

II. SPECT-Volume Processing

The brain SPECT volumes in this study are three-dimensional (3-D) volumes of $128 \times 128 \times d$ size, where d is the depth of the volume, and each horizontal slice is a square of 128×128 pixels. Each pixel is a 16-b value, representing the grey level of brain perfusion at this pixel. A right-handed coordinate system is used in that the x axis increases from left to right, the y axis increases from posterior to anterior, and the z axis increases from inferior to superior. This coordinate system is consistent with the Talairach atlas [15]. The depth d varies from volume to volume; its value is between 48–67 in our experiment. Fig. 1 shows a sample of brain SPECT imaging with coronal, sagittal, and transverse views. Fig. 1(a) is a coronal view in the x–z plane, Fig. 1(b) is a sagittal view in the y–z plane, and Fig. 1(c) is a transverse view in the x–y plane. The intersection of the lines in this sample is the anterior commissure of brain, indicating that the three views are three different viewing planes intersected on this site of brain.

The aim of SPECT-volume processing is to extract useful information from the raw data of the brain SPECT volumes and then provide input–output data pairs to the following fuzzy system. Expert knowledge is exploited to direct the processing. The corpus callosum, situated at the center of the brain, has low perfusion. It is suggested by the radiologist that the transverse views and coronal views around the corpus callosum are analyzed. Then, asymmetry values of a number of regions on these views can be calculated. These asymmetry values can be helpful in distinguishing Tourette's syndrome from chronic tic disorder in children, since Tourette's syndrome is more asymmetric between left and right brains than chronic tic disorder from experts' experiences. Based on this expertise, the input–output data pairs can be obtained through two volume-processing operations: selecting the five data slices around the corpus callosum and obtaining 21 asymmetry values on these five data slices.

A. Selection of Five Data Slices

The top, front, and back slices of the corpus callosum can be automatically found by an auxiliary computer algorithm or manually set by radiologists. The former is used in the experiments of this paper.

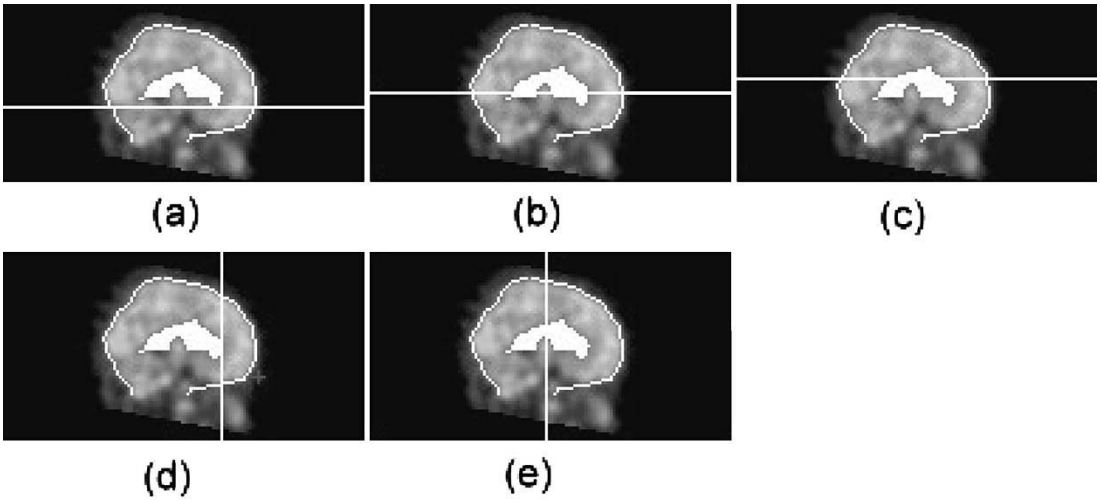

Fig. 2. Five white lines are the five chosen slices around the found corpus callosum of the SPECT sample in sagittal view. (a) Low slice. (b) Middle slice. (c) Upper slice. (d) Frontal slice. (e) Temporal slice.

Since it is auxiliary, due to space constraints, the details of the algorithm are not listed here. In our experiments, the selected slices about the corpus callosum in all volumes were verified by the radiologist. No unacceptable discrepancies in these selected slices between the auxiliary algorithm and the radiologist were found.

After the corpus callosum of brain is found, we can obtain five data slices around the corpus callosum according to the suggestion of the radiologist. Denote d_{low}, d_{middle}, and d_{upper} as the numbering of three chosen transverse slices, and h_{frontal} and h_{temporal} as the numbering of two chosen coronal slices. The selection operation is

$$d_{\text{upper}} = \min(\text{top of the corpus callosum}, d/2 + 5)$$
$$d_{\text{middle}} = d_{\text{upper}} - 5$$
$$d_{\text{low}} = d_{\text{upper}} - 10$$

if (front of the corpus callosum) $>$ (back of the corpus callosum)$+15$, then

$$h_{\text{frontal}} = \min(\text{front of the corpus callosum}, 128/2 + 15)$$

and

$$h_{\text{temporal}} = ((\text{back of the corpus callosum}) + h_{\text{frontal}})/2$$

otherwise

$$h_{\text{frontal}} = (\text{back of the corpus callosum}) + 15$$

and

$$h_{\text{temporal}} = (\text{back of the corpus callosum}) + 7.$$

In Fig. 2, the five white lines are the five selected slices in the sagittal view. The d_{low}, d_{middle}, and d_{upper} slices are approximately on the bottom, the middle, and the top, respectively, of the corpus callosum. Similarly, the h_{frontal} and h_{temporal} slices are approximately on the front and the center, respectively, of the corpus callosum. Fig. 3 shows these five selected slices in the transverse view for the $d_{\text{low}}, d_{\text{middle}}$, and d_{upper} slices and in the coronal view for the h_{frontal} and h_{temporal} slices.

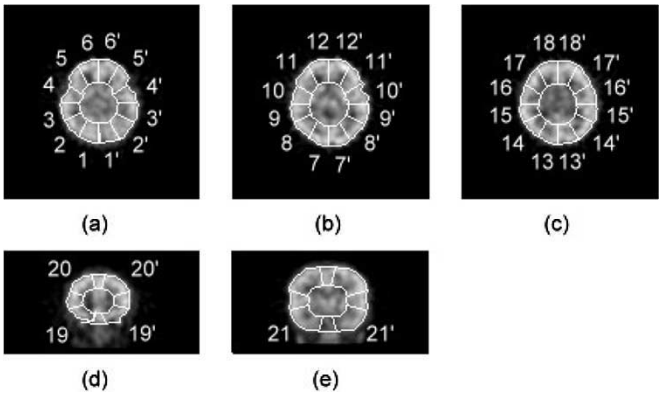

Fig. 3. The 21 left–right regions on the five data slices of the SPECT sample. (a) Low slice. (b) Middle slice. (c) Upper slice. (d) Frontal slice. (e) Temporal slice.

B. Calculation of 21 Asymmetry Volume Data

On the five chosen slices, 21 left–right regions are selected according to the suggestions of the radiologist. The white lines in Fig. 3 show the partitioning of these regions. For the $d_{\text{low}}, d_{\text{middle}}$, and d_{upper} slices, each region is a 30° sector bounded by the outer contour and the half-radius-proportional contour inside brain. Thus, the three transverse slices have 18 left–right regions labeled as in Fig. 3(a), (b), and (c). For the h_{frontal} and h_{temporal} slices, each region is a 60° sector in a quadrant from 15° to 75°, also bounded by the outer contour and the half-radius-proportional contour inside brain. The three left–right regions of these two slices are indicated and labeled in Fig. 3(d) and (e).

The average perfusion value of each left and each right region is calculated. Then, the asymmetry data are given as shown in (1), at the bottom of the page, where i is the numbering of the sample volume.

III. Input-Variables Selection

After the volume processing, 21 asymmetry values in (1) are derived for each SPECT volume. Considering the classification of the two

$$x_i^{(t)} = \frac{(\text{average of left } t \text{ region}) - (\text{average of right } t \text{ region})}{(\text{average of left } t \text{ region}) + (\text{average of right } t \text{ region})}, \quad t = 1, \ldots, 21 \tag{1}$$

classes of Tourette's syndrome and chronic tic disorder, some of these 21 asymmetry variables may not be useful. Principal component analysis (PCA) [16] can be used to obtain feature vectors for a number of the 21-variable data here. However, the feature vectors are many linear combinations of the 21 variables. For human interpretation, it is more desirable to represent the diagnosis operation in terms of individual variables than feature vectors. Thus, PCA is not employed here.

The following algorithm is a heuristic method based on the nearest-neighbor rule in pattern classification [17] to select input variables. If two samples are of the same class, then they are usually closer to each other than two samples of two different classes. In this study, the "closer" here is in terms of Euclidean space. By this consideration, we can check each combination of the 21 asymmetry variables on the two classes of SPECT volumes and obtain a nearness score $\mathrm{near}(S_{\mathrm{sub}})$, S_{sub} being a subset of $\{1,2,\ldots,21\}$, by the following algorithm.

Nearest-Point Algorithm: Let $S_{\mathrm{sub}} \subset S = \{1,2,\ldots,21\}$ be a subset. Denote the input data of the n_1 volumes of the first class as $\boldsymbol{x_1},\ldots,\boldsymbol{x_{n_1}} \in \Re^{\boldsymbol{21}}$, and those of the n_2 volumes of the second class as $\boldsymbol{x_{n_1+1}},\ldots,\boldsymbol{x_{n_1+n_2}} \in \Re^{21}$. Let $\mathrm{near}(S_{\mathrm{sub}})=0$.

Step 1) Construct the reduced input data as $\boldsymbol{x'_1},\ldots,\boldsymbol{x'_{n_1+n_2}} \in \Re^{m'}$, where m' is the size of $S_{\mathrm{sub}} = \{a_1,\ldots,a'_m\}$, and $\boldsymbol{x'_i} = (x_i^{(a_1)},\ldots,x_i^{(a_{m'})})$ is a reduced vector of $\boldsymbol{x_i} = (x_i^{(1)},x_i^{(2)},\ldots,x_i^{(21)})$.

Step 2) For each $\boldsymbol{x'_i}$, calculate the squares of the distances

$$(\boldsymbol{x'_i}-\boldsymbol{x'_j})^T\cdot(\boldsymbol{x'_i}-\boldsymbol{x'_j}),\quad j=1,\ldots,n_1+n_2,\quad j\neq i.$$

Suppose the minimum of the above calculation is for $\boldsymbol{x'_k}$. If $\boldsymbol{x'_i}$ and $\boldsymbol{x'_k}$ belong to different classes, then increase $\mathrm{near}(S_{\mathrm{sub}})$ by 1.

Using this algorithm, the nearness score of any combination of variables can be calculated. However, the combination number is $2^{21}-1$, which is a huge number. In reality, we compute the nearness scores for the cases of one to five variables in our experiment. It is found that few variables can achieve low nearness scores. Then, the combination with the minimum of these scores is used as the input data of the following fuzzy system. One advantage of using only few variables, e.g., less than five, is the interpretation of the resulted smaller-sized fuzzy system. The variables selected through the above algorithm indicate that some regions of the brain show different patterns for Tourette's syndrome and chronic tic disorder. This information can be helpful in distinguishing between these two diseases.

IV. A Fuzzy System With a Two-Step Minimization Approach

A. Characteristic-Point-Based Fuzzy Inference System

Let s be the number of fuzzy rules and m be the dimension of the input $\mathbf{x}$. In this section, we denote the following:

- $m_{\mathrm{in},j}^{(k)}$ centers of the membership functions of the input fuzzy sets, $1\le j\le s, 1\le k\le m$;
- $\sigma_{\mathrm{in},j}^{(k)}$ spreads of the membership functions of the input fuzzy sets, $1\le j\le s, 1\le k\le m$;
- m_j centers of the membership functions of the output fuzzy sets, $1\le j\le s$;
- σ_j spreads of the membership functions of the output fuzzy sets, $1\le j\le s$.

The rule base of a CPFIS is

$$\begin{aligned}&\text{If } x^{(1)} \text{ is } A_1^{(1)} \text{ and}\cdots\text{and } x^{(m)} \text{ is } A_1^{(m)}, \text{then } y \text{ is } B_1\\ &\qquad\vdots\\ &\text{If } x^{(1)} \text{ is } A_s^{(1)} \text{ and}\cdots\text{and } x^{(m)} \text{ is } A_s^{(m)}, \text{then } y \text{ is } B_s\end{aligned}$$

where $A_j^{(k)}$ and $B_j, 1\le j\le s, 1\le k\le m$, are fuzzy sets in the antecedent and consequent parts of fuzzy rules. The membership function of $A_j^{(k)}$ is a bell-shaped function with center $m_{\mathrm{in},j}^{(k)}$ and spread $\sigma_{\mathrm{in},j}^{(k)}$, given as follows:

$$\mu_{A_j^{(k)}}\left(x^{(k)}\right)=\exp\left(-\frac{\left(x^{(k)}-m_{\mathrm{in},j}^{(k)}\right)^2}{2\left(\sigma_{\mathrm{in},j}^{(k)}\right)^2}\right). \tag{2}$$

We call $(m_{\mathrm{in},j}^{(1)},\ldots,m_{\mathrm{in},j}^{(m)}), 1\le j\le s$, CPs. The membership function of B_j is also chosen as a bell-shaped function with center m_j and spread σ_j

$$\mu_{B_j}(y)=\exp\left(-\frac{(y-m_j)^2}{2\sigma_j^2}\right). \tag{3}$$

There are three steps in making an inference of a CPFIS.

Step 1) Calculate the firing strength $w_j, 1\le j\le s$, for each fuzzy rule

$$w_j(\mathbf{x})=\mu_{A_j^{(1)}}\left(x^{(1)}\right)\times\cdots\times\mu_{A_j^{(m)}}\left(x^{(m)}\right). \tag{4}$$

Step 2) Form the output fuzzy sets

$$w_j\mu_{B_j}(y),\quad 1\le j\le s.$$

Step 3) Defuzzify the output fuzzy sets by using the simulated center-of-area method of Lin and Lee [18]

$$y=\frac{\sum_{j=1}^{s} w_j m_j\sigma_j}{\sum_{j=1}^{s} w_j\sigma_j}. \tag{5}$$

The training of CPFIS is to decide the number of fuzzy rules and the parameters of these rules. The following two minimization steps are proposed to perform the training of CPFIS.

The first minimization is based on σ_j. The number of fuzzy rules will be reduced from n, the number of training data, to $s, s\le n$. Then the second minimization is based on $\sigma_{\mathrm{in},j}^{(k)}$. This step is a fine-tuning of parameters in fuzzy sets but not a determination of the number of fuzzy sets. The aim of this fine-tuning is to enhance the precision performance of CPFIS. In Section IV-B, we provide the details of the proposed systematic training process of CPFIS.

B. Gradient-Projection Method

Initially, all training data are mapped to fuzzy rules. The mapping is performed on all data points $(\mathbf{x_i}, y_i), \mathbf{x_i}\in\Re^m, y_i\in\Re$, with $x_i^{(1)},\ldots,x_i^{(m)}$ assigned to be the centers of the membership functions of the input fuzzy sets and y_i assigned to be the centers of the membership functions of the output fuzzy sets. That is

$$\begin{aligned}m_{\mathrm{in},i}^{(t)}&=x_i^{(t)},\quad t=1,\ldots,m,\quad i=1,\ldots,n,\\ m_i&=y_i,\quad i=1,\ldots,n.\end{aligned}$$

Each data point is mapped to a fuzzy rule. Thus, if there are n data points, then initially there are n fuzzy rules. After the mapping, the spreads of the membership functions of the input fuzzy sets $\sigma_{\mathrm{in},j}^{(k)}$ and the spreads of the membership functions of the output fuzzy sets σ_j remain to be set. We set

$$\sigma_{\mathrm{in},j}^{(t)}=\frac{1}{a}\left(\max_{1\le i\le n} x_i^{(t)}-\min_{1\le i\le n} x_i^{(t)}\right),\quad t=1,\ldots,m \tag{6}$$

where a is a chosen constant. In this paper, a is set to be 2. $\sigma_{\mathrm{in},j}^{(k)}$ are the same for all fuzzy rules in this step. They will be different and later fine-tuned in the back-propagation process. The firing strength of a rule j is

$$A(\mathbf{x},\mathbf{x_j})=\exp\left(-\frac{\left(x^{(1)}-x_j^{(1)}\right)^2}{2\left(\sigma_{\mathrm{in},j}^{(1)}\right)^2}-\cdots-\frac{\left(x^{(m)}-x_j^{(m)}\right)^2}{2\left(\sigma_{\mathrm{in},j}^{(m)}\right)^2}\right)$$

TABLE I
MINIMUM SCORES OF THE NEAREST-POINT ALGORITHM APPLIED TO THE 24 SAMPLES

No. of Variables	Combinations	Min. Score (No. of Cases)	Regions of Min. Cases
1	21	8 (2)	(4), (5)
2	210	5 (3)	(3, 5), (4, 9), (9, 14)
3	1330	3 (1)	(8, 12, 20)
4	5985	3 (1)	(4, 6, 8, 20)
5	20349	3 (1)	(2, 3, 5, 14, 19)

and the fuzzy inference output is

$$y = \frac{\sum_{j=1}^{n} y_j \sigma_j A(\mathbf{x}, \mathbf{x_j})}{\sum_{p=1}^{n} \sigma_p A(\mathbf{x}, \mathbf{x_p})}.$$

The weights $\sigma_j, j = 1, \ldots, n$, are initially set to be $1/n$ before the minimization.

After these settings, we can take the training of CPFIS as a constrained minimization problem as follows:

$$\min_{\sigma_1, \ldots, \sigma_n} \sum_{i=1}^{n} \left[y_i - \frac{\sum_{j=1}^{n} y_j \sigma_j A(\mathbf{x_i}, \mathbf{x_j})}{\sum_{p=1}^{n} \sigma_p A(\mathbf{x_i}, \mathbf{x_p})} \right]^2$$
$$\text{subject to} \sum_{j=1}^{n} \sigma_j = 1, \quad \sigma_j \geq 0, \quad j = 1, \ldots, n. \tag{7}$$

A gradient projection method is employed to solve this problem [19]. It is noted that (7) is a general nonlinear equation in the variables $\sigma_1, \ldots, \sigma_n$. Thus, the solution obtained by the gradient-projection method is usually a local minimum.

After the algorithm, many constraints $\sigma_j \geq 0$ become active constraints, i.e., $\sigma_j \approx 0$. The approximation "$\approx$" used here is to take into account the precision of numerical calculations. In the experiments, we label a constraint as an active constraint if σ_j is less than a small positive number. The training data of these active constraints can be removed from being candidates of CPs, since the weights $\sigma_j \approx 0$ of these fuzzy rules are much smaller than those of inactive constraints. It is from the approximation

$$\sum_{i=1}^{n} \left[y_i - \frac{\sum_{j=1}^{n} y_j \sigma_j A(\mathbf{x_i}, \mathbf{x_j})}{\sum_{p=1}^{n} \sigma_p A(\mathbf{x_i}, \mathbf{x_p})} \right]^2 \approx \sum_{i=1}^{n} \left[y_i - \frac{\sum_{j=1}^{s} y_{r(j)} \sigma_{r(j)} A(\mathbf{x_i}, \mathbf{x_{r(j)}})}{\sum_{p=1}^{s} \sigma_{r(p)} A(\mathbf{x_i}, \mathbf{x_{r(p)}})} \right]^2$$

where $r(\cdot)$ is a function that indicates that $r(j)$ is the numbering of the jth fuzzy rules in the original n fuzzy rules. Thus, the indexes of active constraints are not in the output domain of $r(\cdot)$.

C. Back-Propagation Tuning

After the first minimization, there remain $s, s \leq n$, fuzzy rules. The second minimization is based on $\boldsymbol{\sigma}_{\mathbf{in},\mathbf{r(1)}}, \ldots, \boldsymbol{\sigma}_{\mathbf{in},\mathbf{r(s)}}$ as follows:

$$\min_{\boldsymbol{\sigma}_{\mathbf{in},\mathbf{r(1)}}, \ldots, \boldsymbol{\sigma}_{\mathbf{in},\mathbf{r(s)}}} \sum_{i=1}^{n} \left[y_i - \frac{\sum_{j=1}^{s} m_{r(j)} \sigma_{r(j)} A(\mathbf{x_i}, \mathbf{x_{r(j)}})}{\sum_{p=1}^{s} \sigma_{r(p)} A(\mathbf{x_i}, \mathbf{x_{r(p)}})} \right]^2 + \text{regBP} \cdot \sum_{j=1}^{s} \sum_{k=1}^{m} \frac{1}{2 \left(\sigma_{\text{in},r(j)}^{(k)} \right)^2} \tag{8}$$

where $\boldsymbol{\sigma}_{\mathbf{in},\mathbf{r(j)}} = (\sigma_{\text{in},r(j)}^{(1)}, \ldots, \sigma_{\text{in},r(j)}^{(m)})$, and $\text{regBP} > 0$ is a term acting like a regularization parameter. Readers are referred to [16] for the details of the back-propagation process. It is noted that the centers of the membership functions of the input fuzzy sets $\mathbf{m}_{\mathbf{in},\mathbf{r(j)}}$ are not variables in the minimization. We assign $m_{\text{in},r(j)}^{(k)} = x_{r(j)}^{(k)}, k = 1, \ldots, m, j = 1, \ldots, s$. These $\mathbf{x_{r(j)}}$ positions are the obtained CPs from the gradient-projection method.

V. EXPERIMENT AND RESULTS

To test the performance of the proposed method, experiments were conducted on 17 SPECT volumes of Tourette's syndrome and 7 SPECT volumes of chronic tic disorder from National Cheng Kung University Hospital, Tainan, Taiwan, R.O.C. All 24 volumes are for pediatric patients. The imaging device is a triple-headed rotating gamma camera (Multispect3; Siemens, Hoffman Estates, USA). The experiments were performed on a Pentium III PC with a 600-MHz CPU and 128 MB memory. The operating system is Windows ME. Except for the nearest-point algorithm, Java was used to implement the proposed method and the programming software is JBuilder 4. The 24 volumes have been used in investigating the differences in perfusion between Tourette's syndrome and chronic tic disorder in [20]. Although the number of samples is not large, it is generic to some extent.

A. SPECT-Volume Processing

All 24 volumes were first processed by the volume processing as described in Section II. The five data slices around the corpus callosum were obtained, and the 21 input data were calculated for each volume.

B. Input-Variables Selection

The nearest-point algorithm of Section III was then applied to the obtained 21-input–1-output data. Table I lists the minimum scores of the algorithm for the combinations of one to five variables. The case of three variables has the minimum score of 3 and a smaller number of variables than other cases; therefore, we took the three variables for Regions 8, 12, and 20 of the minimum-score case as the input variables of the fuzzy system. We used MATLAB version 6.1 of the PC version to run the algorithm. The total of the cases is $C_1^{21} + C_2^{21} + C_3^{21} + C_4^{21} + C_5^{21} = 27\,895$, where C_m^n denotes the number of combinations in selecting m elements from n elements. The running time was 1121.3 s on the same experiment PC.

C. Construction of CPFIS

After the nearest-point algorithm, we had the training data of 24 cases of three input variables and one output variable. The output was set to 1 for Tourette's syndrome and -1 for chronic tic disorder. The gradient-projection method was applied to these 24 training data to obtain CPs. Initially, the spreads of the output fuzzy membership function σ_j was set to be $1/n = 1/24$. The parameter a in (6) was set to be 2. The threshold of σ_j was set to be 10^{-8}. If any σ_j was less than this threshold, then $\sigma_j \approx 0$. Thus, from (7), $\sigma_j \approx 0$ became an active constraint. The corresponding training data for this active constraint, $\sigma_j \approx 0$, were removed from the candidate CPs. Initially, all 24 training data were all candidates, but after 200 epochs of the gradient-projection algorithm, there only 7 candidates remained. The running time of the gradient-projection method was 12.85 s for the Java program on the experiment PC.

The back-propagation tuning was then used to minimize (8) based on $\sigma_{\text{in},r(j)}^{(k)}$. The parameter regBP in (8) was set to 10^{-6}. The learning

TABLE II
PARAMETERS OF THE FUZZY RULES IN THE TRAINED FUZZY SYSTEM

Rule	$m_{in,r(j)}^{(1)}$, $m_{in,r(j)}^{(2)}$, $m_{in,r(j)}^{(3)}$ [a]	$\sigma_{in,r(j)}^{(1)}$, $\sigma_{in,r(j)}^{(2)}$, $\sigma_{in,r(j)}^{(3)}$ [b]	$m_{r(j)}$ [c]	$\sigma_{r(j)}$ [d]
j=1	-0.04459, -0.07246, -0.01149	0.00948, 0.07165, 0.00901	1	0.15432
j=2	0.04490, -0.04280, -0.02878	0.01085, 0.06956, 0.00463	1	0.09347
j=3	-0.01923, -0.07077, -0.02898	0.04695, 0.05336, 0.00098	1	0.01113
j=4	-0.05628, -0.04681, -0.00685	0.01059, 0.06906, 0.01246	1	0.11842
j=5	-0.03311, 0.06849, 0.02251	0.05179, 0.03017, 0.00388	1	0.37753
j=6	0.0, -0.04120, 0.02532	0.03675, 0.01224, 0.00315	-1	0.14839
j=7	-0.01370, 0.01370, -0.01676	0.02258, 0.01314, 0.00434	-1	0.09674

[a] $m_{in,r(j)}^{(m)}$: Centers of the input membership functions.
[b] $\sigma_{in,r(j)}^{(m)}$: Spreads of the input membership functions.
[c] $m_{r(j)}$: Centers of the output membership functions.
[d] $\sigma_{r(j)}$: Spreads of the output membership functions.

rate η and momentum constant α were set to 0.2 and 0.95, respectively. The back-propagation learning was performed with 10 000 epochs. It took 6.65 s for the Java program on the experiment PC.

After the construction of CPFIS, we obtained 7 fuzzy rules for all 24 volumes. Table II lists the trained parameters of the seven fuzzy rules. The training error is $\sum_{j=1}^{24}(y(\mathbf{x_j}) - y_j)^2 = 0.2613$, where $y(\mathbf{x_j})$ and y_j denote the outputs of CPFIS and the actual outputs from training data, respectively. The minimum case of Tourette's syndrome is $\min_{1\le j\le 17} y(\mathbf{x_j}) = 0.759$, and the maximum case of chronic tic disorder is $\max_{18\le j\le 24} y(\mathbf{x_j}) = -0.708$. In the experiment, if $y(\mathbf{x_j}) \ge 0$, the sample was diagnosed as Tourette's syndrome; contrarily, if $y(\mathbf{x_j}) < 0$, the sample was diagnosed as chronic tic disorder. Thus, the two classes were correctly recognized by the trained CPFIS.

Fig. 4 shows the membership functions of the input and output fuzzy sets of these seven rules. In the figure, the first five rules are for Tourette's syndrome, while the last two are for chronic tic disorder. These fuzzy rules can be roughly described as follows.

- Rule 1) If x (region 8) is *negative*, x (region 12) is *negative*, and x (region 20) is *zero*, then it is Tourette's syndrome.
- Rule 2) If x (region 8) is *positive*, x (region 12) is *negative*, and x (region 20) is *negative*, then it is Tourette's syndrome.
- Rule 3) If x (region 8) is *zero*, x (region 12) is *negative*, and x (region 20) is *negative*, then it is Tourette's syndrome.
- Rule 4) If x (region 8) is *negative*, x (region 12) is *negative*, and x (region 20) is *zero*, then it is Tourette's syndrome.
- Rule 5) If x (region 8) is *negative*, x (region 12) is *positive*, and x (region 20) is *positive*, then it is Tourette's syndrome.
- Rule 6) If x (region 8) is *zero*, x (region 12) is *negative*, and x (region 20) is *positive*, then it is chronic tic disorder.
- Rule 7) If x (region 8) is *zero*, x (region 12) is *zero*, and x (region 20) is *zero*, then it is chronic tic disorder.

The x variable here denotes the asymmetry value of each left–right region as in (1). It is noted that the terms "zero," "positive," and "negative" are only fuzzy sets for each rule to describe the positions of them in each rule. They are not the same across these fuzzy rules. A fuzzy set is labeled as "zero," "positive," or "negative" if the center of it is between -0.02 and 0.02, greater than or equal to 0.02, or less than or equal to -0.02, respectively. The linguistic description accompanied with the graphical representation of these seven rules is a useful medium to summarize the underlying mechanism of the CAD.

Clinically, it is observed in many patients that the cerebral cortical perfusion of the left brain is lower than that of the right brain for Tourette's syndrome. On the contrary, the cerebral cortical perfusion is more symmetric between the left and right brains for chronic tic disorder. Rule 1 of Fig. 4 matches the above observation that, if x (Region 8) and x (Region 12) are negative, then it is Tourette's syndrome. On the other hand, Rule 7 of Fig. 4 matches the symmetry of chronic tic disorder that, if x (Region 8), x (Region 12), and x (Region 20) are zero, then it is chronic tic disorder.

If the most firing rules for these 24 volumes are listed, Rule 1 is the most firing rule for eight volumes of Tourette's syndrome, while Rule 7 is the most firing rule for four volumes of chronic tic disorder. Therefore, they are the most important rules for diagnosing the two diseases. The other five rules have fewer cases and may be related to minor clinical observations different from the above major property of Tourette's syndrome and chronic tic disorder.

If only two rules, Rules 1 and 7, were used in the CPFIS, two volumes of Tourette's syndrome and two volumes of chronic tic disorder were misclassified. The accuracy was 83.3% (20 of 24). Hence, Rules 1 and 7 are the two main and effective rules in the operation of the CPFIS.

D. Leave-One-Out Test

To test the proposed system on the cases not used in the training set, leave-one-out tests were performed. That is, one volume is excluded during the training on all the other volumes and then diagnosed by the trained fuzzy system. The leave-one-out tests were repeated eleven times for a in (6) to be $2.0, 2.1, \ldots, 3.0$, and the accuracies were 79%, 79%, 71%, 67%, 71%, 67%, 67%, 71%, 75%, 75%, and 71%, respectively. The mean and standard deviation of the accuracies were 72.0% and 4.6%, respectively. Hence, a was set to be 2 for its 79% accuracy performance in this paper.

To decide the threshold between Tourette's syndrome and chronic tic disorder, the receiver operating characteristic (ROC) curve [21] was evaluated by using the ROCKIT provided by C. Metz at the University of Chicago. Fig. 5 shows the ROC curve for the leave-one-out test of the (8, 12, 20)-variables case. The area under the ROC curve, A_z, is 0.8158. The threshold of 0.0 approximately at the center of the ROC curve was chosen in the rest of this paper. The A_z value is not more than 0.9. Thus, a combination of the CPFIS and the radiologist is provided in the follows.

Table III shows the performance of the leave-one-out test when $a = 2$ and the diagnosis result by the radiologist (Nan-Tsing Chiu, MD). Region 8 is posterior parietal in transverse slices, region 12 is anterior frontal in transverse slices, and region 20 is orbitofrontal in coronal slices. These regions are on single slices, but left frontal (LF) and others in the second column of Table III are specific brain areas which are at many slices.

Of these 24 cases, the radiologist correctly classified the seven volumes of chronic tic disorder, but did not recognize 3 volumes

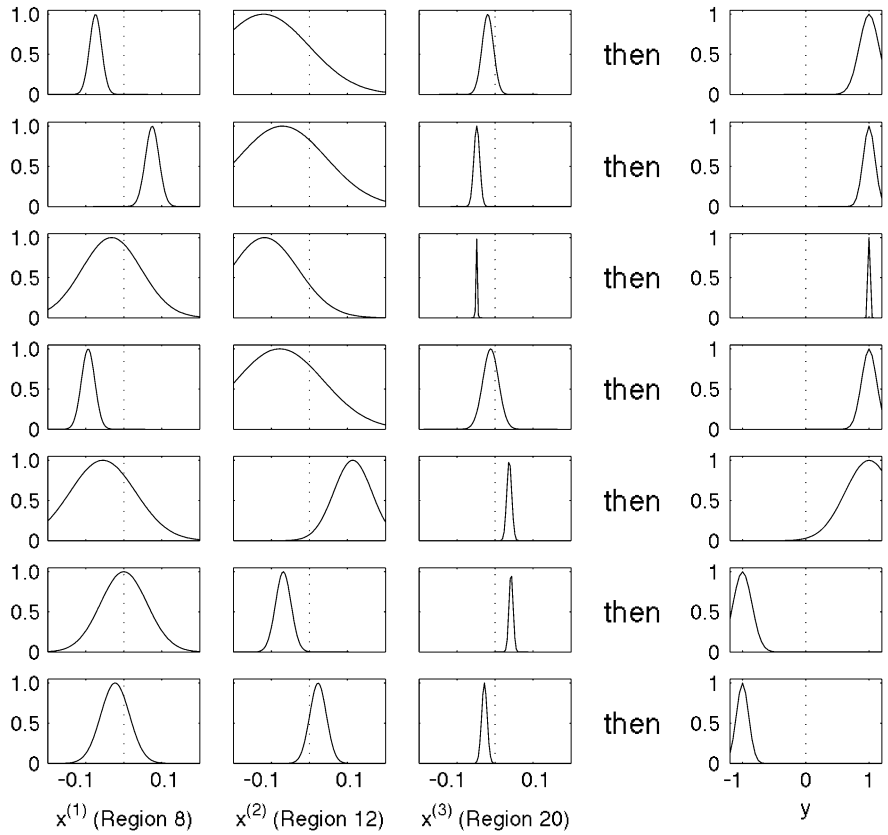

Fig. 4. Seven fuzzy rules of the proposed system. The first five rules are for Tourette's syndrome, while the last two are for chronic tic disorder. The three input variables are from regions 8, 12, and 20 of the data slices.

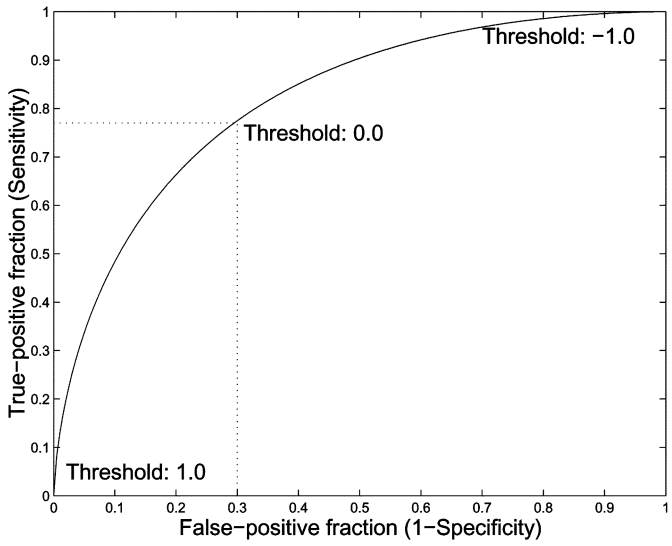

Fig. 5. Diagram of the ROC curve for the leave-one-out test of the (8, 12, 20)-variables case. The A_z value for the ROC curve is 0.8158.

of Tourette's syndrome by visual interpretation of cerebral cortical perfusion. The radiologist and the CPFIS had different results in eight cases. In particular, cases 5, 7, and 12, which were misclassified by the radiologist, were correctly diagnosed by the CPFIS. Thus, the CPFIS can provide a useful second-reader opinion to the radiologist. For example, if one case was diagnosed as chronic tic by the radiologist but as Tourette's syndrome by the CPFIS, then this case could be taken as Tourette's syndrome. By so doing, all 17 cases of Tourette's syndrome were correctly diagnosed with two chronic tic cases being misdiagnosed. The accuracy of the radiologist increased from 87.5% (21 of 24) without the CPFIS to 91.7% (22 of 24) with the CPFIS. If Tourette's syndrome is labeled as positive and chronic tic disorder is labeled as negative in the two-class diagnosis, sensitivity and specificity can be calculated. The sensitivity of the radiologist increased from 82.4% (14 of 17) without the CPFIS to 100% (17 of 17) with the CPFIS, but the specificity decreased from 100% (7 of 7) without the CPFIS to 71.4% (5 of 7) with the CPFIS. Since Tourette's syndrome is more severe than chronic tic, early detection and treatment for the patients of Tourette's syndrome is important. The CPFIS can complement the radiologist and help find the cases of Tourette's syndrome without too many misdiagnosed cases of chronic tic disorder.

Using McNemar's test for significant changes [22], the changes of the accuracy performances for the radiologist before and after the above combination with the CPFIS is not statistically significant $(\chi^2 = 0.05, df = 1, P > 0.05)$. However, the correlation coefficient between the radiologist's diagnosis and the CPFIS is only 0.2988. In the experiment of the 24 samples, the CPFIS can provide different but effective information to the radiologist. The CPFIS based on regions 8, 12, and 20 and the simple linguistic terms *positive*, *negative*, and *zero* employed in its operation provide another set of information to the radiologist. It is noted that Tourette's syndrome has a 2:1 prevalence relation with respect to tic cases. Thus, the aforementioned combination is biased toward Tourette's syndrome. Without more clinical examinations, the radiologist accepted the suggestion from the combined diagnosis in this research. Although the construction and application process of the proposed method is complete in this research, the small sample size of 24 does not allow the results to be directly applied to general Tourette's syndrome and chronic tic

TABLE III
COMPARISON OF THE RESULTS OF THE RADIOLOGIST AND THE CPFIS IN THE 24 CASES

Volume	Radiologist		CPFIS		Diff.
	Findings[a]	Diag.	Major Rule[b]	Diag.	
Tourette no. 1	LF, LT	Tourette	$x(8)$N, $x(12)$N, $x(20)$Z	Tourette	No
Tourette no. 2	LF	Tourette	$x(8)$Z, $x(12)$Z, $x(20)$Z	Chronic tic	Yes
Tourette no. 3	LF, LT	Tourette	$x(8)$P, $x(12)$Z, $x(20)$N	Tourette	No
Tourette no. 4	LF	Tourette	$x(8)$P, $x(12)$N, $x(20)$N	Chronic tic	Yes
Tourette no. 5		Chronic tic	$x(8)$N, $x(12)$N, $x(20)$Z	Tourette	Yes
Tourette no. 6	LB	Tourette	$x(8)$Z, $x(12)$Z, $x(20)$Z	Tourette	No
Tourette no. 7		Chronic tic	$x(8)$N, $x(12)$P, $x(20)$P	Tourette	Yes
Tourette no. 8	LF	Tourette	$x(8)$N, $x(12)$P, $x(20)$P	Tourette	No
Tourette no. 9	LF, LT, LB	Tourette	$x(8)$N, $x(12)$N, $x(20)$Z	Tourette	No
Tourette no. 10	LF, LT	Tourette	$x(8)$N, $x(12)$N, $x(20)$Z	Tourette	No
Tourette no. 11	LF	Tourette	$x(8)$N, $x(12)$N, $x(20)$Z	Tourette	No
Tourette no. 12		Chronic tic	$x(8)$N, $x(12)$P, $x(20)$Z	Tourette	Yes
Tourette no. 13	LF, LT	Tourette	$x(8)$N, $x(12)$N, $x(20)$Z	Tourette	No
Tourette no. 14	LB	Tourette	$x(8)$Z, $x(12)$N, $x(20)$P	Chronic tic	Yes
Tourette no. 15	LT, LTh	Tourette	$x(8)$N, $x(12)$P, $x(20)$P	Tourette	No
Tourette no. 16	RT, RB	Tourette	$x(8)$N, $x(12)$N, $x(20)$Z	Tourette	No
Tourette no. 17	LF	Tourette	$x(8)$N, $x(12)$N, $x(20)$Z	Tourette	No
Chronic tic no. 1		Chronic tic	$x(8)$Z, $x(12)$N, $x(20)$N	Tourette	Yes
Chronic tic no. 2		Chronic tic	$x(8)$Z, $x(12)$N, $x(20)$P	Chronic tic	No
Chronic tic no. 3		Chronic tic	$x(8)$Z, $x(12)$Z, $x(20)$Z	Chronic tic	No
Chronic tic no. 4		Chronic tic	$x(8)$Z, $x(12)$N, $x(20)$Z	Chronic tic	No
Chronic tic no. 5		Chronic tic	$x(8)$Z, $x(12)$Z, $x(20)$Z	Chronic tic	No
Chronic tic no. 6		Chronic tic	$x(8)$Z, $x(12)$Z, $x(20)$Z	Chronic tic	No
Chronic tic no. 7		Chronic tic	$x(8)$N, $x(12)$N, $x(20)$Z	Tourette	Yes

[a]L: left, R: right, T: temporal, Th: thalamus, F: frontal, B: basal ganglion. The listed items indicate that low perfusion is found in these areas.
[b]$x(8)$: x(region 8), $x(12)$: x(region 12), $x(20)$: x(region 20), P: *positive*, N: *negative*, Z: *zero*.

disorder. To apply to general cases, more samples should be used and tested in order to design a universally effective CAD without small-sample-size concerns.

E. Comparison With PCA

PCA is a standard dimensionality reduction technique for signal representation [23]. For comparisons with the nearest-point algorithm, PCA was also tried to obtain effective input variables. The MATLAB command, **princomp**, was used to perform PCA on the original 24×21 data. Then, the 21 new variables obtained for the 24 SPECT volumes were used in the construction of CPFIS. The relationship between the original variables and the new variables is

$$\left(\mathbf{x_i^T} - \mathbf{m^T}\right) \cdot \mathrm{PC} = \mathbf{x_{i,new}^T}, \quad i = 1, 2, \ldots, 24$$

where $\mathbf{x_i}$ is the original 21×1 data vector, $\mathbf{m}$ is the mean vector of $\mathbf{x_i}$, PC is a 21×21 matrix of 21 principal components, and $\mathbf{x_{i,new}}$ is the new 21×1 data vector. For example, if only the first principal component is used, then

$$x_{i,\mathrm{new}}^{(1)} = \left(\mathbf{x_i^T} - [0.0122, -0.0064, \ldots, -0.0207]\right) \cdot [-0.4755, -0.181\,97, \ldots, 0.389\,55]^T.$$

The explained variances for the first ten new variables were 25.5%, 18.6%, 10.4%, 9%, 7.5%, 5.8%, 4.6%, 4.5%, 2.9%, and 2.9%, respectively. Since in the nearest-point algorithm the numbers of variables were from one to five, the first five new variables from PCA were used for comparison. Table IV shows the performances of different selections of variables after the leave-one-out tests. The first eight rows are the minimum-score cases from the nearest-point algorithm as in Table I, the next five rows are the cases of the five largest explained-variance variables from PCA, and the last row is the application of the nearest-neighbor rule. Except for the last one, each case was run seven times at $a = 2.0, 2.5, 3.0, 3.5, 4.0, 4.5$, and 5.0, respectively. The best accuracy performance among these seven tries for each case is recorded in Table IV.

In the table, the three cases (8, 12, 20), (4, 6, 8, 20), and (2, 3, 5, 14, 19) from the nearest-point algorithm have better or equal performances than the five PCA cases. If **corrcoef** of MATLAB was used to calculate the correlation coefficient between the second and fourth columns in the table, the value is -0.8459. Therefore, the nearest score has somewhat indirect relationship to accuracy. This indicates that approximately if the nearest score is lower, the accuracy is better [22]. In the 24 samples of this research, PCA does not provide better performance than the proposed nearest-point algorithm. In fact, examples are

TABLE IV
PERFORMANCE COMPARISON WITH PCA FOR THE 24 SAMPLES

Method (Variables)	Nearest Score[a]	a[b]	Accuracy	Sensitivity	Specificity
(4)	8	2.0	70.8%	100%	0%
(5)	8	2.0	70.8%	100%	0%
(3, 5)	5	2.0	70.8%	100%	0%
(4, 9)	5	4.5	75%	88.2%	42.9%
(9, 14)	5	4.0	83.3%	94.1%	57.1%
(8, 12, 20)	3	2.0	79.2%	82.4%	71.4%
(4, 6, 8, 20)	3	4.5	75%	88.2%	42.9%
(2, 3, 5, 14, 19)	3	4.0	79.2%	88.2%	57.1%
PCA (1)	5	2.0	70.8%	100%	0%
PCA (1, 2)	5	2.0	75%	100%	14.3%
PCA (1, 2, 3)	8	3.5	58.3%	76.5%	14.3%
PCA (1, 2, 3, 4)	8	4.0	54.2%	70.6%	14.3%
PCA (1, 2, 3, 4, 5)	12	2.5	66.7%	88.2%	14.3%
NN Rule[c]	16	-	33.3%	35.3%	28.6%

[a] $near(S_{sub})$ in Section III.
[b] a in (6).
[c] The nearest neighbor rule with Euclidean distance [17].

provided in [23] to point out that PCA is good for signal representation, but not necessarily good for pattern recognition.

If the nearest-neighbor rule [17] with Euclidean distance was used to classify the 24 samples in the leave-one-out test, the accuracy was 33.3%, as shown in the last row of Table IV. This demonstrates that the employed Euclidean distance does not apply to the nearest-neighbor rule. Although the covariance matrix of the samples can be used to represent better distances for the nearest-neighbor rule, the number of 23 samples in the leave-one-out test are not enough to construct effective covariance matrices [23].

In the table, the variables (4, 6, 8, 20) and (2, 3, 5, 14, 19) are totally different but with the same nearest score, 3. This can be partly accounted for by the correlation coefficients between these variables which are shown at the bottom of the page. The five pairs 4-2, 4-3, 6-14, 8-5, and 20-19 in bold face have nonzero correlation. Therefore, in view of the nearest-point algorithm, the employments of (4, 6, 8, 20) and (2, 3, 5, 14, 19) have similar effects.

The case of variables (9, 14) in the fifth row of the table exhibits a better accuracy performance than that of variables (8, 12, 20). However, if it is combined with the radiologist as described in the last subsection, the accuracy is 87.5%, which is not better than the accuracy performance of the radiologist without the CPFIS. Therefore, the variables (8, 12, 20) were used to construct the CPFIS of this research.

VI. CONCLUSION

In this paper, a fuzzy system, CPFIS, is proposed to help radiologists perform CAD of Tourette's syndrome and chronic tic disorder in children. Early differential diagnosis between these two childhood-onset diseases is difficult but important because early treatment can improve the child's condition. Two volume-processing operations were first applied to SPECT volumes: selecting the five data slices around the corpus callosum and calculating 21 asymmetry values for the 21 left–right regions on the five data slices for each volume. Then effective variables were chosen from these 21 variables by a nearest-point algorithm. The original volume data were thus reduced to the training data of fewer input variables, which were more suitable for two-class diagnosis. Then a two-step minimization approach, consisting of a gradient-projection method and a back-propagation tuning, was employed on the training data to construct the fuzzy system. Experiment results show that the built CPFIS has two major fuzzy rules that match the major patterns of Tourette's syndrome and chronic tic disorder in perfusion imaging. The mean and standard deviation of the accuracies in 10 leave-one-out tests of different parameters were 72.0% and 4.6%, respectively. If one case was diagnosed as chronic tic by the radiologist but as Tourette's syndrome by the CPFIS, then this case could be taken as Tourette's syndrome. By so doing, all 17 cases of Tourette's syndrome were correctly diagnosed with two chronic tic cases being misdiagnosed. The accuracy of the radiologist increased from 87.5% (21 of 24) without the CPFIS to 91.7% (22 of 24) with the CPFIS. Since Tourette's syndrome is more severe than chronic tic, early detection and treatment for the patients of Tourette's syndrome is important. The CPFIS can provide an effective second-reader opinion in finding the cases of Tourette's syndrome. It is noted that Tourette's syndrome has a 2:1 prevalence relation with respect to tic cases. Thus, the employed combined diagnosis is biased toward Tourette's syndrome. Although the construction and application process of the proposed method is complete in this research, the small sample size of 24 does not allow

---

4-2: $\mathbf{-0.54}$, 4-3: $\mathbf{0.57}$, 4-5: -0.08, 4-14: 0.04, 4-19: 0.09,
6-2: 0.03, 6-3: 0.11, 6-5 : -0.25, 6-14: $\mathbf{-0.24}$, 6-19: 0.09,
8-2: 0.36, 8-3: 0.00, 8-5: $\mathbf{0.41}$, 8-14: 0.31, 8-19: -0.05,
20-2: -0.26, 20-3: 0.04, 20-5: -0.01, 20-14: -0.01, 20-19 : $\mathbf{0.31}$

the results to be directly applied to general Tourette's syndrome and chronic tic disorder. To apply to general cases, more samples should be used and tested in order to design a universally effective CAD without small-sample-size concerns.

REFERENCES

[1] G. L. Clementz, R. H. Lee, and A. M. Barclay, "Tic disorders of childhood," *Am. Family Physician*, vol. 38, no. 2, pp. 163–170, Aug. 1988.

[2] D. J. Lacey, "Diagnosis of Tourette syndrome in children. The need for heightened awareness," *Clin. Pediatrics*, vol. 25, no. 9, pp. 433–435, Sept. 1986.

[3] K. Kompoloti and C. G. Goetz, "Hyperkinetic movement disorders misdiagnosed as tics in Gilles de la Tourette syndrome," *Movement Disorders*, vol. 13, no. 3, pp. 477–480, May 1998.

[4] V. Eapen and M. M. Robertson, "All that tics may not be Tourette's," *Br. J. Psychiatry*, vol. 164, no. 5, p. 708, May 1994.

[5] J. Moriarty, V. Eapen, D. C. Costa, S. Gacinovic, M. Trimble, P. J. Ell, and M. M. Robertson, "HMPAO SPET does not distinguish obsessive-compulsive and tic syndromes in families multiply affected with Gilles de la Tourette's syndrome," *Psychol. Med.*, vol. 27, pp. 737–740, 1997.

[6] K. G. Sieg, D. Buckingham, G. R. Gaffney, D. F. Preston, and K. G. Sieg, "Tc-99m HMPAO SPECT brain imaging of Gilles de la Tourette's syndrome," *Clin. Nucl. Med.*, vol. 18, no. 3, p. 255, 1993.

[7] J. L. Lampreave, V. Molina, M. J. Mardomingo, A. Bittini, P. Dominguez, I. Almoguera, F. J. Rubia, and J. L. Carreras, "Technetium-99m-HMPAO in Tourette's syndrome on neuroleptic therapy and after withdrawal," *J. Nucl. Med.*, vol. 39, no. 4, pp. 624–628, Apr. 1998.

[8] I. Gordon, "Cerebral blood flow imaging in paediatrics: A review," *Nucl. Med. Commun.*, vol. 17, pp. 1021–1029, 1996.

[9] P. S. Klieger, K. A. Fett, T. Dimitsopulos, and R. Kurlan, "Asymmetry of basal ganglia perfusion in Tourette's syndrome shown by Technetium-99m-HMPAO SPECT," *J. Nucl. Med.*, vol. 38, no. 2, pp. 188–191, Feb. 1997.

[10] J. Moriarty, D. C. Costa, B. Schmitz, M. R. Trimble, P. J. Ell, and M. M. Robertson, "Brain perfusion abnormalities in Gilles de la Tourette's syndrome," *Br. J. Psychiatry*, vol. 167, pp. 249–254, 1995.

[11] H. D. Cheng, Y. M. Lui, and R. I. Freimanis, "A novel approach to microcalcification detection using fuzzy logic technique," *IEEE Trans. Med. Imag.*, vol. 17, pp. 442–450, June 1998.

[12] S. Yu and L. Guan, "A CAD system for the automatic detection of clustered microcalcification in digitized mammogram films," *IEEE Trans. Med. Imag.*, vol. 19, pp. 115–126, Feb. 2000.

[13] M. G. Penedo, M. J. Carreira, A. Mosquera, and D. Cabello, "Computer-aided diagnosis: A neural-network-based approach to lung nodule detection," *IEEE Trans. Med. Imag.*, vol. 17, pp. 872–880, Dec. 1998.

[14] T. K. Yin and N. T. Chiu, "An interactive bone-scintigraphy diagnosis by a characteristic-point-based fuzzy inference system," in *Proc. 6th Conf. Artificial Intelligence and Applications*, Kao-hsiung, Taiwan, Nov. 2001, pp. 652–657.

[15] J. Tailairach and P. Tournoux, *Coplanar Stereotaxic Atlas of the Human Brain*. New York: Thieme, 1988.

[16] S. Haykin, *Neural Networks: A Comprehensive Foundations*. Piscataway, NJ: IEEE Press, 1994.

[17] T. M. Cover and P. E. Hart, "Nearest neighbor pattern classification," *IEEE Trans. Inform. Theory*, vol. IT-13, pp. 21–27, Jan. 1967.

[18] C. T. Lin and C. S. G. Lee, "Neural-network-based fuzzy logic control and decision system," *IEEE Trans. Comput.*, vol. 40, pp. 1320–1336, Dec. 1991.

[19] D. G. Luenberger, *Linear and Nonlinear Programming*, 2nd ed. Reading, MA: Addison-Wesley, 1989.

[20] N. T. Chiu, Y. C. Chang, B. F. Lee, C. C. Huang, and S. T. Wang, "Differences in 99mTc-HMPAO brain SPET perfusion imaging between Tourette's syndrome and chronic tic disorder in children," *Eur. J. Nucl. Med.*, vol. 28, no. 2, pp. 183–190, Feb. 2001.

[21] C. E. Metz, "ROC methodology in radiologic imaging," *Invest. Radiol.*, vol. 21, pp. 720–733, 1986.

[22] D. S. Phillips, *Basic Statistics for Health Science Students*. San Francisco, CA: Freeman, 1978.

[23] K. Fukunaga, *Introduction to Statistical Pattern Recognition*, 2nd ed. New York: Academic, 1990.

Correction to "Effect of Skull Resistivity on the Spatial Resolutions of EEG and MEG"

S. Martinoia*, P. Massobrio, M. Bove, and G. Massobrio

In [1], we stated, "The NEURON and GENESIS software packages are available free of charge and have never been commercially distributed." These programs have never been distributed commercially; they have always been available free of charge.

REFERENCES

[1] S. Martinoia, P. Massobrio, M. Bove, and G. Massobrio, "Cultured neurons coupled to microelectrode arrays: circuit models, simulations and experimental data," *IEEE Trans. Biomed. Eng.*, vol. 51, pp. 859–864, May 2004.

Manuscript received May 4, 2004. *Asterisk indicates corresponding author*.

*S. Martinoia is with the Neuroengineering and Bio-nanoTechnology Group, Department of Biophysical and Electronic Engineering, University of Genova, Via Opera Pia 11a, 16145 Genova, Italy (e-mail: giaser@dibe.unige.it).

P. Massobrio is with the Neuroengineering and Bio-nanoTechnology Group, Department of Biophysical and Electronic Engineering, University of Genova, 16145 Genova, Italy (e-mail: Paolo.Massobrio@ingegneria.studenti.unige.it).

M. Bove is with the Department of Experimental Medicine, Section of Human Physiology, University of Genova, 16132 Genova, Italy (e-mail: bove@dibe.unige.it).

G. Massobrio is with the Neuroengineering and Bio-nanoTechnology Group, Department of Biophysical and Electronic Engineering, University of Genova, 16145 Genova, Italy (e-mail: biofet@dibe.unige.it).

Digital Object Identifier 10.1109/TBME.2004.832417